Nanoscale Electron Transport and Photodynamics Enhancement in Lipid-Depleted Bacteriorhodopsin Monomers

Sabyasachi Mukhopadhyay,[†,‡] Sidney R. Cohen,[§] Debora Marchak,[†] Noga Friedman,[‡] Israel Pecht,[∥] Mordechai Sheves,[‡,*] and David Cahen[†,*]

[†]Department of Materials and Interfaces, [‡]Organic Chemistry, [§]Chemical Research Support, and [∥]Immunology, Weizmann Institute of Science, Rehovot, Israel 76100

ABSTRACT Potential future use of bacteriorhodopsin (bR) as a solid-state electron transport (ETp) material requires the highest possible active protein concentration. To that end we prepared stable monolayers of protein-enriched bR on a conducting HOPG substrate by lipid depletion of the native bR. The ETp properties of this construct were then investigated using conducting probe atomic force microscopy at low bias, both in the ground dark state and in the M-like intermediate configuration, formed upon excitation by green light. Photoconductance modulation was observed upon green and blue light excitation, demonstrating the potential of these monolayers as optoelectronic building blocks. To correlate protein structural changes with the observed behavior, measurements were made as a function of pressure under the AFM tip, as well as humidity. The junction conductance is reversible under pressure changes up to ~300 MPa, but above this pressure the conductance drops irreversibly. ETp efficiency is enhanced significantly at >60% relative humidity, without changing the relative photoactivity significantly. These observations are ascribed to changes in protein conformation and flexibility and suggest that improved electron transport pathways can be generated through formation of a hydrogen-bonding network.

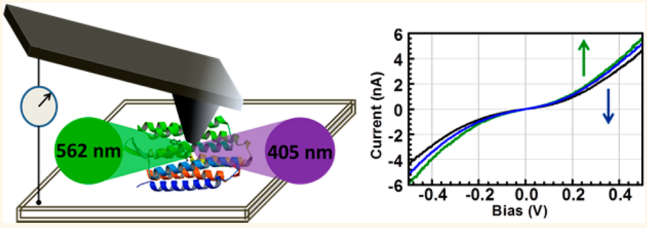

KEYWORDS: bacteriorhodopsin · molecular conductance · conducting atomic force microscopy · electron transport · bimolecular optoelectronics

Bacteriorhodopsin (bR) is a light-driven proton-pumping membrane protein with seven trans-membrane helical structures, arranged in a 2D hexagonal lattice, usually found in crystalline purple membrane patches (PM), used by *Halobacterium salinarum* to convert absorbed light to chemical energy.[1−3] In bR, light absorption initiates vectorial proton transport from the cytoplasmic (CP) to the extracellular (EC) sides of the membrane and has been used to convert light to electrochemical (proton gradient) energy.[4,5] The retinal chromophore, embedded in the ion channel of each bR monomer, is responsible for reversible light-induced trans-membrane proton transport, which results in coordinated molecular motions and electrostatic interactions, commonly known as the photocycle.[6] Upon light excitation, the retinal in the all-trans configuration is isomerized to 13-cis and forms, *via* several intermediates, a blue-shifted M intermediate, which relaxes thermally back to the ground state within a few milliseconds.[7] Besides the retinal photoisomerization, which is a key event in the proton pumping process, the photocycle is also associated with conformational rearrangement of the surrounding protein structure.[8,9] The lifetime of the M intermediate can be externally altered by different methods, such as pressure, blue light illumination, relative humidity, pH, temperature, site-directed mutagenesis, and surrounding electrostatic environment.[10−12]

Its dramatic light-induced structural effect, which leads to photoswitching and photochromism, suggests that bR can serve as an excellent biomaterial for constructing bio(opto)electronic devices in diverse technological areas. Electronic transport (ETp) in wild-type and different variants of bR has already been studied as dry patches, either in its native PM environment or embedded

* Address correspondence to mudi.sheves@weizmann.ac.il; david.cahen@weizmann.ac.il.

Received for review January 13, 2014 and accepted July 8, 2014.

Published online July 08, 2014
10.1021/nn500202k

in a pseudomembrane.[13,14] The results are consistent with tunneling and hopping as the dominating transport mechanisms at low (<160 K) temperatures and higher temperatures, respectively.[13,15−17] In all these experiments, ETp was probed along the vectorial direction of the proton pump channel. Thus, the longitudinal (long) trans-membrane axis, along which the light-induced proton-translocation activity of bR occurs, also was likely the axis of the measured electronic conduction. Macroscopic solid-state junctions prepared on PM monolayer patches (native lipidated bR) revealed nonlinear *I*−*V* characteristics and photostimulated enhanced conduction upon green light illumination ($\lambda >$ 500 nm).[16,18,19] The retinal moiety significantly affects electron transport *via* both wild-type (WT) and bR variants, based on the order of magnitude lower currents that flow if the retinal−protein covalent bond is eliminated, which partially removes the chromophore from its natural binding site (apo-bR).

Nanoscale and large-area measurements on cysteine-modified PM variants (M163C and Q3C) from which the lipids were mostly removed (delipidated) confirmed that ETp is *via* the protein, rather than *via* the lipid layer in which it is embedded in PM.[17,20−23]

It was found that in a hydrated environment delipidated bR still maintains the complete photocycle, involving the same intermediates as in its native PM.[24] Still, delipidation does change the photodynamics of bR by retarding thermal relaxation of the photochemically induced M-intermediate to the ground state.[25] In order to use higher protein concentrations that should enhance electrical conduction across bR-containing monolayers, we probed ETp across partially lipid-depleted WT-bR (delipidated bacteriorhodopsin, dLbR), where ∼70% of the PM lipids were removed with the aid of a gentle detergent treatment.[26] dLbR was immobilized as a monolayer, taking advantage of interactions of the WT surfaces, normally in contact with lipids, with the surface of highly ordered pyrolytic graphite (HOPG) as conducting substrate. ETp of the immobilized dLbR was investigated as a function of applied force, excitation wavelength, and relative hydration levels.

RESULTS AND DISCUSSION

The dLbR monolayer on HOPG was characterized by tapping mode AFM imaging, with minimal force (95% of oscillation amplitude, average force <500 pN) applied to the monolayer. Topographic images with different amplitude set points confirm that the monolayers are densely packed with an approximate average height of 2 nm, instead of 5 nm along the protein's longitudinal axis, as expected and as was observed earlier for immobilized lipidated bR on different substrates (SI, Figure S1).[13] High-resolution crystal structure studies of bR indicate that each monomeric α-helix has a diameter of ∼2.6−2.9 nm (SI, Figure S2).[27] *Based on the above observation, we postulate that dLbR is immobilized by hydrophobic interactions along its long dimension with HOPG and is in its monomeric form*. This is possible if dLbR, which retains its trimer configuration in solution, separates into monomers upon adsorption onto the hydrophobic HOPG surface, possibly driven by hydrophobic and $\pi-\pi$ stacking interactions between the hydrophobic body of the protein, previously buried inside the PM, and HOPG.

Sample characterization by FTIR spectroscopy reveals spectral broadening and blue shift of the α-helical amide I band of the monomeric dLbR monolayer on HOPG, compared to that of a drop-cast multilayer film (SI, Figure S3a). The shift to lower energy in the FTIR spectra indicated that at least part of the lipids that hold the trimers together were released.[26] Spectral broadening may result from chemical interaction between the surface-exposed hydrophobic amino acids on the α-helical dLbR monomer structure and the HOPG surface.[28] In addition to FTIR, UV−vis absorption spectra of the dLbR-monomer monolayer and multilayers show the characteristic absorption band (∼560 nm), suggesting that the protein did not experience a major structure alteration even in the dry delipidated monomeric configuration. (SI, Figure S3b).

ETp properties of monomeric dLbR were characterized by conducting probe AFM (CP-AFM), which allows acquiring information on ETp efficiencies as a function of tip force applied to the monolayer (Figure 1). The effect of increasing force is to increase the contact area and contact stiffness, as well as the penetration depth. As reviewed recently,[29] the analytical equations that describe the relations between applied force and pressure under the AFM probe presume a geometrically well-defined tip and homogeneous/isotropic surface. For our AFM measurements on thin films and monomeric protein molecules, these assumptions cannot be made, and a new approach to calculate applied pressure effects is detailed in the SI.

ETp measurements were carried out by bringing a freshly cleaned Pt-coated Si probe into mechanical contact with the dLbR monolayer on HOPG. Even with the asymmetric device structure (small-tip electrode and large-area substrate), *I*−*V* characteristics at minimal applied force (∼5−10 nN) are rather symmetrical (with slight deviations only at large applied forces) around zero bias, which is also consistent with an effective superohmic nature ($I \propto V^2$) of the contacts. At fixed bias voltage, deviations in current magnitude (20−30%) between different junctions were observed, which could be attributed to a variation in applied force (±1−2 nN) and especially to variation in the areal density of dLbR monomers over the examined regions (SI, Figure S1e and f).

The effect of applied force on ETp across a monomeric dLbR monolayer was examined by analyzing

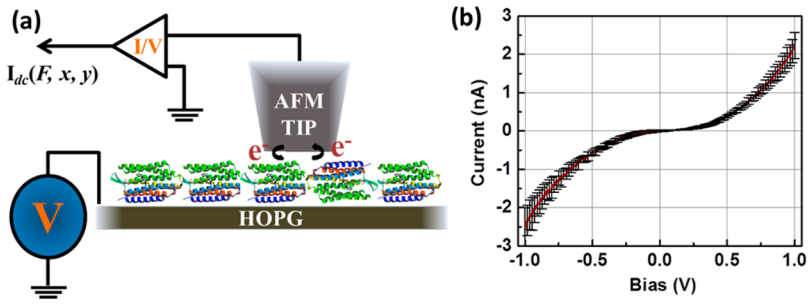

Figure 1. (a) Schematic of electron transport measurement across a dLbR monolayer with conducting probe atomic force microscopy. (b) The result of statistically averaging *I*−*V* characteristics of a typical dLbR junction on a HOPG substrate at moderate applied force (~8 nN); horizontal bars represent the variation in current magnitude over 50 successive measurements.

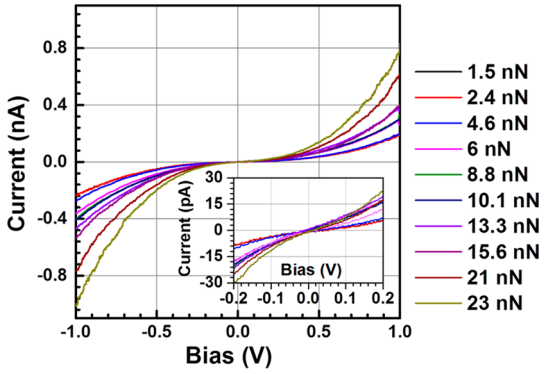

Figure 2. Influence of applied force on *I*−*V* behavior (average of ~50 measurements, error is ±50 pA at 0.5 V) of a dLbR monolayer on a HOPG substrate at room temperature at 4% relative humidity. Inset: *I*−*V* curves at low bias voltages.

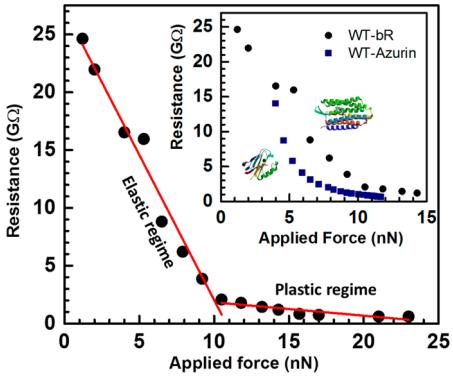

Figure 3. Variation of dLbR junction resistances (average of 50 measurements) with applied forces as measured with a Pt-coated AFM probe after immobilization on a HOPG substrate. Two different force regimes are clearly observed. (Inset) Force-dependent electrical responses for azurin (β-sheet structure) (from ref 33) and dLbR (α-helical structure).

changes in the *I*−*V* curves as a function of the applied force on a given junction. Typical *I*−*V* curves of dLbR junctions, obtained in the dark at various specific loads, are shown in Figure 2. At forces less than 1 nN, junction currents were below our detection limit (1 pA). With increasing applied forces, a monotonic enhancement in junction current was observed up to 30 nN. For forces greater than 40 nN, a drastic increase in current magnitude was observed, which probably originates from AFM-probe penetration through the soft dLbR monolayer (SI, Figure S4). Force-dependent electronic conduction across monomeric bR was obtained by monitoring the changes in low voltage conductance (*G*), which is estimated from the slope of the *I*−*V* curves for $|V| \leq 0.1$ V (inset in Figure 2). The conductance variation with the applied force can be divided into two ranges (Figure 3), an elastic one (2−10 nN, where changes in conductance with force are reversible) and a plastic one (>10 nN, where an irreversible process takes place as bR does not regain its initial conductance).

According to our calculations, described in the SI (section 4), 10 nN corresponds to a pressure of slightly less than 300 MPa. This pressure is orders of magnitude above the several kPa pressures, which lead to conformational changes in bR in solution, affecting the photocycle.[10] Similarly, the corresponding contact stiffness is 2−3 orders of magnitude higher than the force constant deduced for the purple membrane.[30] In these referenced works a lipid-containing membrane was measured, and presumably then a very different structural change was probed than the intraprotein deformation probed here. Thus, we have no direct reference for comparison to deduce what structural changes may occur in dLbR under these conditions. However, pressure-related hydration changes were recently observed to occur on four different representative proteins at 200 MPa pressure.[31] This may give a clue to the nature of structural changes occurring here, as well as to the sensitivity to humidity levels (*vide infra*).

In the elastic regime (lower applied pressure), the 2.5 GΩ/nN slope likely represents the resistance variation due to increasing contact area with pressure, as well as contributions of additional transport paths that can be accessed, and/or decreasing contact resistance, at higher pressure. The magnitude and functional behavior of this dependence can be rationalized with the elastic model (Hertzian contact) outlined in the SI. Within that model the change in contact radius varies with the force to the power 1/3, and the spreading resistance varies inversely with contact radius,

yielding a sublinear dependence of resistance on force. Thus, adding this to the additional conductance paths which can develop with pressure, could lead to the linear dependence observed. The shorter tunneling path contributes only in a minor way to increased current. Using the elastic model described in the SI, and presuming an exponential increase of current with deformation, with an ETp length decay constant of ~0.2 $Å^{-1}$,[17] the resistance should decrease only 2-fold upon increasing applied force from 1.5 nN to 10 nN, as compared with the 10-fold decrease observed in Figure 3.

Following the linearization approximation of nondiodic systems (over a range of ±0.1 V around zero bias), we estimate the resistivity of the dLbR monolayer from the observed slope at around 5 nN force (see SI, section 4) and find it to be approximately 10^5 Ω-cm, similar to that of clean silicon (without intentional doping) at room temperature. In the plastic regime (10−30 nN) the (now irreversible) enhancement in conductance with applied force is smaller (slope 0.1 GΩ/nN). We attribute this behavior to significant alteration(s) in protein conformation and structure, which *no longer represents the bR WT configuration*.

The electrical conductance across monomeric dLbR along its transverse short axis is 2 orders of magnitude higher (1−2.5 nS at 10 nN) than that observed over a PM monolayer on Au (~20−60 pS at 10 nN). It corresponds to an electron transfer decay constant (β) value of dLbR ≈ 0.17 $Å^{-1}$ before correcting for the different lipid concentrations and is similar to the β (0.15 $Å^{-1}$) value as obtained with a Cytochrome 562 mutant that could be and was chemically bound to the contacting electrodes *via* a cysteine group on each side, in both standing-up and lying-down configurations (with the protein dimension that dictates the separation between the electrodes being 5 and 2.3 nm, respectively).[32] Previous studies with proteins in a solid-state configuration yielded $\beta = 0.12$ $Å^{-1}$ for lipidated WT-bR and 0.15 $Å^{-1}$ for azurin.[13,14] The higher current magnitude can be attributed to the lower concentration of insulating lipids in the dLbR than in the PM monolayer and to the much shorter junction length of the dLbR than the PM junction (~2 nm *vs* >5 nm). The change in current magnitude over the force range used is similar to that found with azurin, a known electron transfer protein, immobilized on a gold-coated substrate.[33] Azurin, with its β-sheet secondary structure, shows mechanical flexibility under applied force in the force range used here and exhibits a *reversible* decrease in junction resistance with applied force (inset in Figure 3). Monomeric dLbR, with the stiffer α-helical structure and, thus, higher mechanical stability, shows both reversible and irreversible responses over the force range.

To check if a monomeric dLbR monolayer still maintains photoactivity, similar to that of bR in its natural environment, ETp under green (λ 562 nm) and blue (λ 405 nm) illumination was measured. Specific wavelengths were chosen based on the known bR-photocycle characteristics and the optical absorption spectrum of the dLbR monolayer. In these experiments, the probe was engaged at 6−8 nN in the dark to give stable electrical contact, after which steady-state ETp characteristics were measured, giving G_{dark}. Measurements were then repeated under continuous green light illumination, yielding G_{green}, where $G_{green} > G_{dark}$. The effect of green illumination on ETp decayed thermally to close to the G_{dark} value after turning off the green light (SI, Figure S5). Over the applied force range G_{green} was approximately 1.4−2 times G_{dark} (SI, Figure S6). Multiple successive measurements were carried out on a single junction, without withdrawing the tip, over illumination cycles with a period of 15−30 s. This results in a G_{green} modulation that is typically reproducible over three full cycles.

If, instead of green, blue illumination is used, we do not find any conductance enhancement over the examined force range (SI, Figure S7). This result suggests that the green illumination indeed excites the retinal chromophore in dLbR monomers and that the green illumination-induced increased junction conductance ($\Delta G = G_{green} - G_{dark}$) can be associated with formation of the photochemically induced M-like intermediate.[11,16,18,23,34,35] To support this interpretation, blue light was *added* to the green light illumination, which reduced the current magnitude in *I*−*V* curves (Figure 4). Previously, measurements with near-field scanning optical microscopy of lipidated bR monolayers on a quartz substrate (at ambient humidity) demonstrated that the fraction of the M-like intermediate states is reduced upon adding blue on top of green light illumination.[35,36] During successive green and (blue + green) illumination cycles, a reproducible conductance variation was observed over typically three to four full cycles (Figure 5). While the relative change in the green light-induced conductance ($\Delta G/G_{dark}$) varies between junctions (SI, Figure S6 inset), the conductance under blue-green co-illumination was consistently reduced (for 90% of the junctions, probed), compared to that obtained with green illumination only. These observations rule out junction heating upon illumination as the cause of the conductance changes and strongly support the interpretation that during green light illumination the photochemically induced M-like intermediate (absorbing around 410 nm) is accumulated and increases the conductance. Addition of blue light decreases the conductance, because the blue light excites mainly the M-like intermediate and shortens its lifetime, thus accelerating its conversion back to the initial dark bR state and decreasing its fraction in the mixture of M-like intermediate and ground (dark) state.[11]

The higher current flow at a given bias in the green illumination-induced M-like state can be associated with the stronger H-bonding network in this state than

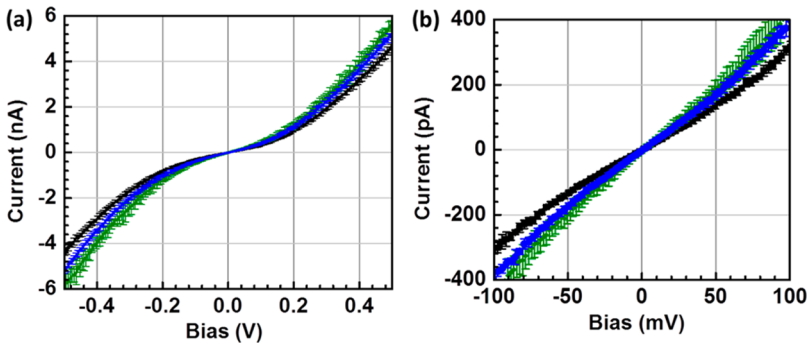

Figure 4. Typical light-induced conduction modulation of a dLbR junction. (a) *I*−*V* characteristics of a dLbR junction in the dark (black), under green illumination (green), and with blue + green illumination (blue). (b) *I*−*V* curves at low bias voltage; linear fits to these curves are used to calculate conductance values of dLbR junctions under different illumination conditions. A 6−8 nN tip force was used to ensure stable contacts over time.

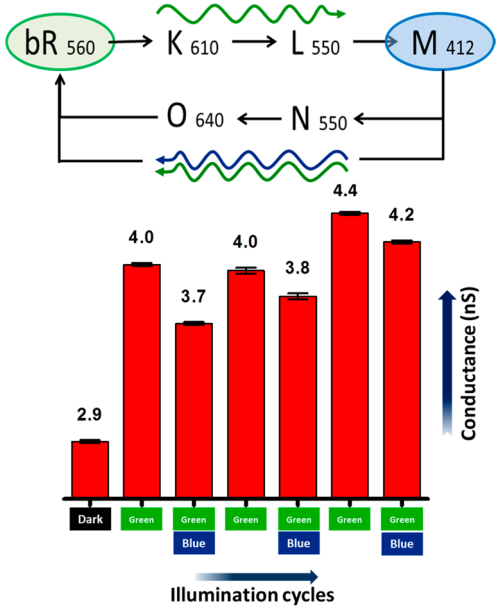

Figure 5. Conductance modulation of a dLbR junction, following bR photoexcitation. (Top) Schematic of bR photocycle; (bottom) modulated junction conductance (numbers on top of bars, in nS) under different illumination conditions (shown at bottom).

in the dark bR state, which may lower the activation energy for transport. We note that green light-induced enhanced conductance is consistent with recently reported ETp studies on PM monolayers in macroscopic junctions and also with CP-AFM measurements (with an applied tip force of 12−15 nN) on partially delipidated bR variants that were attached *via* a cysteine residue to a gold substrate.[23,37] The photoinduced conductance enhancement and modulation demonstrate that delipidated bR monomers still retain their photochemical activity.

In the photoinduced M-like intermediate state, junction resistance also monotonically decreases with applied force, as is seen for measurements of a dLbR monomer in the ground state (dark condition; with only AFM feedback laser, $\lambda \approx 680$ nm) (SI, Figure S8a). The conductance of dLbR monomer junctions was significantly enhanced under green light illumination compared to that in the dark, as long as junctions were probed with an applied force within the elastic force range (2−10 nN), *i.e.*, the green illumination-induced relative conductance change, $G_{green}/G_{dark} \cong 2$ (*i.e.*, $\Delta G/G_{dark} \cong 1$). When junctions were probed in the plastic force range, $\Delta G/G_{dark}$ reduces to as little as 0.2 (SI, Figure S8b). Our findings indicate that even though dLbR monomers conduct better in the intermediate M-like state than in its ground (dark) state, in the elastic regime the force-dependent ETp of dLbR monomer in both states is similar. Thus, in the elastic force range there is no force dependence of the *relative* photoconductance, induced by green illumination, while $\Delta G/G_{dark}$ decreases monotonically with force in the plastic regime.

We interpret this behavior as follows: at low forces, there is efficient conversion of the ground state to the M-like intermediate under green illumination and minor dLbR monomer structural perturbation. At higher forces, in the plastic range, dLbR monomers are accessed by higher applied force, which hinders the light-induced conformational changes and impedes M-like state formation, leading to a decrease in photoconductivity.[38]

The results described above were obtained at a relative humidity (RH) of 4%, in which dry, solid-state-like dLbR monomers, similarly to PM membranes,[30] probably contain only tightly bound water molecules. It allows the protein to retain a conformation that resembles the native one (as indicated by the retained absorption, FTIR, and photoactivity). In the case of lipidated bR, the amount of M-intermediate accumulated under steady-state illumination and the thermal relaxation of the M-intermediate to the ground state are mainly determined by the specific hydration state of the membrane.[39−41] Our earlier studies of PM in macroscopic junctions (lipidated bR monolayers in standing-up configuration on a substrate) showed less efficient ETp at 85% than at lower relative humidity. The finding can be ascribed to formation of a water monolayer on the

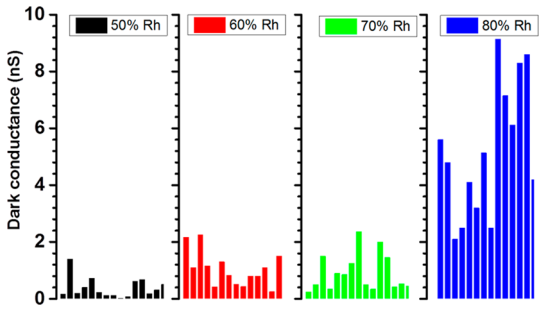

Figure 6. Distributions of dLbR dark junction conductance values in the different humidity conditions, shown at the top.

hydrophilic extracellular and cytoplasmic ends of the bR, which are the ends that serve as contact areas in that measurement configuration; therefore, the presence of such a layer reduces conductivity.[17]

Water molecules inside the native bR structure are inhomogeneously distributed in two separate regions: (i) less dense molecules, trapped inside the retinal cavity and surrounding the proton channel, and (ii) diffuse water molecules, concentrated near the extracellular and cytoplasmic sites.[42] To shed further light on the effect of the hydration level on ETp *via* monomeric dLbR monolayer junctions, we carried out transport measurements over the relative humidity range from 4% to 85% (at 6−8 nN applied force above the adhesion force, which was found to be constant at ~2 nN over the full humidity range, SI, Figure S9). Before electrical measurements, samples were kept in a dry N_2 environment at 4% humidity, so as to remove residual water molecules and allow uniform water distribution inside the dLbR monolayer. As humidity increases, water absorbed by the monomers affects the conformation and flexibility and consequently the ETp across the monomeric dLbR monolayer. Upon increasing the relative humidity, the electrical conductance of dLbR junctions in the ground state at low bias ($|V| \leq 0.1$ V) increases moderately. The rather wide distribution of dark conductance values for different dLbR junctions complicates humidity-dependent ETp comparisons. Thus, we compare the statistically averaged conductance that was measured over 30−40 junctions at each humidity level. Figure 6 represents the statistically distributed dark conductance of different dLbR junctions measured under different relative humidities.

Force−distance curves show negligible change in their slope indicating no change in film compliance over the humidity range examined (Figure S9); at relative humidities greater than 90% all the junctions electrically shorted, likely because the large number of absorbed water molecules that diffused into the interior of the protein made the dLbR films more flexible and softer. A monotonic increase in average conductance was observed when varying the humidity from 4% to 60%, with a sharp jump for humidity exceeding 70%. This ETp increase may be due to better contact or because electrical pathways become more efficient. Recent studies on PM demonstrate that even at very low humidity a few water molecules remain bound near the retinal and the proton channel.[42] In PM, the amount of associated water molecules grows progressively up to 80% relative humidity and then increases sharply, which can be attributed to the above-mentioned water layer formation on its naturally exposed surfaces and possibly also to a drastic change in water distribution in the protein interior,[43] as a shell of water was shown, for oligothiophene, to be able to affect electron transport drastically.[44] In contrast, at higher humidity (>20%) the water molecules adsorbed on monomeric dLbR monolayers are unlikely to hinder conduction between protein and electrodes, as they do not accumulate on the monolayer surface, because of the hydrophobic nature of that surface, which, in the PM, is surrounded by lipids. It has been hypothesized that hydration affects the environment of the retinal and induces conformational changes of the protein, which may impact the retinal−protein interaction and electron transport properties.[42] Such hydration-induced conformational changes are expected to induce formation of internal hydrogen bonding and induce p*K* shifts of terminal amino acids.[45,46]

Interestingly, with the electrodes that we use that are only electronically conducting, we find at higher humidities, where the PM is more hydrated and known to facilitate proton pumping, enhanced electronic conduction through dLbR junctions. The enhanced conductance at higher humidity suggests a possible relation between proton transfer and ETp, in which H-bonded water molecules may serve to mediate between proton and electronic transport activity of bR.[47]

CONCLUSIONS

We explored the potential of monomeric bR, obtained by extracting bR from its membrane environment, as an optoelectronic material, using solid-state ETp studies of dLbR monomer junctions under different applied forces and relative humidities, in the dark and under different illuminations. In a solid-state configuration, dLbR monomer in its photoinduced intermediate M-like state is a more efficient electronic transport medium than in its dark-adapted ground state. We suggest that structural alteration of the hydrated M-like intermediate state facilitates electronic transport compared to the ground state. Above 35% relative humidity water molecules start interacting with hydrophobic parts of amino acids, generating intraprotein H-bonding and increasing the intraprotein network of hydrogen bonding. This network, *via* structured water, may facilitate electron conduction. In this way water molecules, which themselves have poor electronic conduction, may help to mediate electronic transport, as was proposed for tunneling pathways in

electron transfer proteins.[47] The intraprotein hydrogen-bonding network, produced in the hydrated state, enhances retinal chromophore interaction with proton translocation pathways in the protein backbone.[43,48] This phenomenon may also cause humidity-dependent ETp, a notion that we are currently investigating. Force-dependent ETp variations show that there is an optimal pressure condition where the dLbR monolayer appears to be a rather efficient photoaddressable transport medium. dLbR monolayers can be considered as a photoswitchable biomaterial for solid-state current-carrying electronic elements that can be integrated in bioelectronic device structures. Our findings emphasize the building-block potential of dLbR by extracting bR from its membrane environment and relating to it as a molecular unit, probing it in its monomeric state.

MATERIALS AND METHODS

dLbR Preparation. Suspended purple membrane solution (concentrated) was incubated overnight with magnetic stirring with a mild detergent, CHAPS (3-[(3-cholamidopropyl)-dimethylammonio]-1-propanesulfonate), and phosphate buffer (pH 6). This detergent treatment partially (~70%) delipidates the membrane and produces an aqueous solution of bR trimers, which are kept together by endogenous lipids. Finally, the solution was centrifuged to clean the product as a monodispersed concentrated solution.

dLbR Monolayer Preparation. The HOPG surface was cleaned by freshly cleaving with Scotch tape before protein incubation. Special care was taken regarding the quality, homogeneity, and flatness of the HOPG surface. A 200 μL droplet of WT-type delipidated bR suspension in phosphate buffer at pH 6 was deposited on the HOPG surface and incubated for 6−7 h in a vibration-free enclosure (sometimes under a N_2 atmosphere), followed by rinsing in phosphate buffer and Milli-Q water (18 Ω) and drying under a stream of N_2 gas. Until measurement, samples were kept in a custom-made inert atmosphere (Ar)-filled chamber overnight to obtain a dry monolayer. The immobilization driving forces rely mainly on hydrophobic and π-stacking interactions between the exposed (surface) hydrophobic and aromatic side chain residues of bR and the π-delocalized hydrophobic HOPG surface. The result, after finding the right incubation parameters (80 μM concentration of dLbR in the buffer) and incubation time, is a densely packed monolayer of monomeric bR with an overall average height of ~2 nm [confirmed by AFM topography], which agrees with the short dimension of the transversal axis of a bR monomer.

AFM Imaging. The topography of the immobilized dLbR proteins was characterized by AFM in semicontact mode under constant N_2 flow purge (4% relative humility). Solver P47 (NT-MDT, Zelenograd, Russia) and Multimode/Nanoscope-V (Bruker-Nano, Santa Barbara, CA, USA) SPM systems were used in combination with Pt-coated Si probes (SNC18, 15 kHz, 0.2 N/m; 80 kHz, 2.8 N/m from Mikromasch). Topography and phase images were obtained simultaneously at a scan rate of 1 Hz. During the semicontact scans, the average force, applied to the protein monolayer, was 1−2 orders of magnitude below that used for the contact-probe measurements. The formation of a protein monolayer with ~70% coverage on the HOPG substrate was confirmed by comparing topographic and phase images, obtained in semicontact mode with different amplitude reduction or amplitude set point ratio as described in ref 33.

Optical and Structural Characterization. To ensure protein functionality in this dry state (dry in the sense that only tightly bound water molecules remain), IR measurements were performed on drop-cast dry films and monolayers of dLbR. This characterization is of prime importance, as biological function is closely related to the structure of bR and also because of changes in protein structure, which can significantly influence electron transport characteristics. For dry films the PM-IR-RAS technique was used, while for the monolayers G-ATR was employed to enhance the signal-to-noise ratio. IR measurements on films show the expected amide I and amide II peaks at positions of 1665 and 1547 cm^{-1}, respectively. A spectral broadening and small shift of the amide I peak (1655 cm^{-1}) and the amide II peak (1547 cm^{-1}) were observed for the monolayer. These changes can be attributed to small changes in the alpha-helices, presumably arising from those helices that interact with the surface during immobilization. UV−vis absorption spectroscopy on dLbR monolayers was performed with a photoluminescence quantum yield apparatus. The spectrum shows a strong absorption feature at around 560 nm, which represents the ground-state absorption that initiates the light-induced bR photocycle.

Electrical Transport Measurement. Electron transport measurements through a dLbR monolayer were performed by CP-AFM, as a function of applied force and relative humidity with an environment-controlled Solver P47 (NT-MDT, Zelenograd, Russia) SPM system. The 680 nm AFM-feedback laser was active for all the experiments. At that wavelength bR has negligible absorbance. Also, control measurements without a feedback laser demonstrate no significant change in $I-V$ curves. Pt-coated Si probes (SNC18, 15 kHz, 0.2 N/m and SNC20, 75 kHz, 2 N/m) were used for the conduction measurements. The AFM probes were brought into contact with the protein monolayer using constant force feedback (contact mode). The applied force on the protein monolayer was obtained from the precalibrated distance-deflection sensitivity curves of each AFM probe over the examined humidity range. The applied force is in addition to the small adhesive force (~2 nN), which was constant over the humidity range studied (see SI section 9). During the measurement, the electrical stability of each junction was first probed by scanning from −0.5 V to +0.5 V at a rate of 0.2 s^{-1}. The electrical quality of the junction was analyzed following the symmetric nature of the $I-V$ curves along the voltage axis. Fifty $I-V$ curves were acquired at a rate of 0.2 s^{-1} and statistically averaged for each junction. Finally curves with less than 10% variation at 0.5 V were considered for further electrical conduction and electron transport analysis. A tip force of 4−7 nN was used to obtain stable $I-V$ curves with high signal-to-noise ratio and to avoid any change of protein secondary structure.

Relative humidity inside the environmentally isolated chamber was controlled by constant dry N_2 purging through an aqueous bubbler, where the flow rate was computer controlled *via* an electronic feedback loop to control the RH with a precision of 5% in the 4% to 60% RH range and of 10% in the 60% to 90% RH range (humidity sensor, Honeywell, HM4000 series). Each examined junction was illuminated with optically collimated green (562 nm, 5 mW) and blue (405 nm, 10 mW) laser light separately or together (co-illumination), using a mechanical chopper to allow lock-in detection. Illumination was through a glass optical window (T 94% at an angle of 20°) of the environment chamber. With this setup we obtained $I-V$ curves between 4% and 85% RH under different optical illumination conditions. Force-dependent photoresponse measurements with green illumination (Figure S8) demonstrate that the largest light effect can be achieved only at a lower tip force (~2−3 nN). A strong green light effect was obtained at 3 nN tip force at ±1 V as shown in Figure S5a. Because of tip stability in longer experiments with blue-green illumination, measurements were performed at limited bias voltage and at a force of 6−8 nN (Figure 4), as results were not reproducible at lower force (~3 nN).

For each relative humidity, $I-V$ measurements were performed only after the system stabilized and remained stable for 3 h. During measurements at higher humidity, the accumulation of a water layer on the dLbR monolayer was carefully examined,

using the force–distance curves (including capillary adhesion in the force) on the unexposed area of the HOPG substrate and on the dLbR layer, followed by transport measurements at very low applied force (1.5 nN). For each sample, around 20 junctions were probed over a scan area of $1 \times 1\ \mu m^2$ and statistically averaged for each relative humidity. Before each conduction measurement on a monolayer junction, the probe quality was checked by verifying that an electrical short was formed on the bare HOPG surface. The AFM probe was cleaned from time to time, using voltage pulses (+10 to −10 at a rate of 50 s^{-1}).

Conflict of Interest: The authors declare no competing financial interest.

Supporting Information Available: Tapping mode AFM characterization of immobilized dLbR monomers on a HOPG substrate; high-resolution bR structure and distance between helical structures (cartoon representation from PyMOL software, PDB code 1R2N); FTIR and UV–vis characterization of a monomeric dLbR monolayer; discussion on force-dependent conductance; characterization of photoinduced dLbR monomer junction modulation with green illumination; distribution of dark junction conductance and corresponding green-illumination-induced conductance enhancement; effect of blue light illumination; force-dependent relative resistance variation of a dLbR monomer junction at ground state and M-intermediate configuration; force-deflection profiles under different humidity conditions; relative-humidity-dependent light responses are provided. This material is available free of charge *via* the Internet at http://pubs.acs.org.

Acknowledgment. We thank the Minerva Foundation (Munich), the Kimmelman Center for Biomolecular Structure and Assembly, and the Kimmel Center for Nanoscale Science for partial support. S.M. thanks the Council for Higher Education (Israel) for a PBC program postdoctoral research fellowship. M.S. holds the Ephraim Katzir/Rao Makineni Professorial Chair of Chemistry. D.C. holds the Schaefer Chair in Energy Research.

REFERENCES AND NOTES

1. Henderson, R.; Unwin, P. N. T. Three-Dimensional Model of Purple Membrane Obtained by Electron Microscopy. *Nature* **1975**, *257*, 28–32.
2. Oesterhelt, D.; Stoeckenius, W. Rhodopsin-like Protein from the Purple Membrane of Halobacterium halobium. *Nat. New Biol.* **1971**, *233*, 149–152.
3. Lanyi, J. K. Bacteriorhodopsin. *Annu. Rev. Physiol.* **2004**, *66*, 665–688.
4. Lanyi, J. Proton Transfer and Energy Coupling in the Bacteriorhodopsin Photocycle. *J. Bioenergy Biomembr.* **1992**, *24*, 169–179.
5. Zimanyi, L.; Varo, G.; Chang, M.; Ni, B.; Needleman, R.; Lanyi, J. K. Pathways of Proton Release in the Bacteriorhodopsin Photocycle. *Biochemistry* **1992**, *31*, 8535–8543.
6. Varo, G.; Lanyi, J. K. Thermodynamics and Energy Coupling in the Bacteriorhodopsin Photocycle. *Biochemistry* **1991**, *30*, 5016–5022.
7. Ye, T.; Friedman, N.; Gat, Y.; Atkinson, G. H.; Sheves, M.; Ottolenghi, M.; Ruhman, S. On the Nature of the Primary Light-Induced Events in Bacteriorhodopsin: Ultrafast Spectroscopy of Native and C_{13}=C_{14} Locked Pigments. *J. Phys. Chem. B* **1999**, *103*, 5122–5130.
8. Sass, H. J.; Gessenich, R.; Koch, M. H. J.; Oesterhelt, D.; Dencher, N. A.; Büldt, G.; Rapp, G. Evidence for Charge-Controlled Conformational Changes in the Photocycle of Bacteriorhodopsin. *Biophys. J.* **1998**, *75*, 399–405.
9. Lanyi, J. K.; B, S. Crystallographic Structure of the Retinal and the Protein after Deprotonation of the Schiff Base: The Switch in the Bacteriorhodopsin Photocycle. *J. Mol. Biol.* **2002**, *321*, 727–737.
10. Klink, B. U.; Winter, R.; Engelhard, M.; Chizhov, I. Pressure Dependence of the Photocycle Kinetics of Bacteriorhodopsin. *Biophys. J.* **2002**, *83*, 3490–3498.
11. Ohno, K.; Govindjee, R.; Ebrey, T. G. Blue Light Effect on Proton Pumping by Bacteriorhodopsin. *Biophys. J.* **1983**, *43*, 251–254.
12. Dencher, N. A.; Sass, H. J.; Büldt, G. Water and Bacteriorhodopsin: Structure, Dynamics, and Function. *Biochim. Biophys. Acta, Bioenerg.* **2000**, *1460*, 192–203.
13. Ron, I.; Pecht, I.; Sheves, M.; Cahen, D. Proteins as Solid-State Electronic Conductors. *Acc. Chem. Res.* **2010**, *43*, 945–953.
14. Ron, I.; Sepunaru, L.; Itzhakov, S.; Belenkova, T.; Friedman, N.; Pecht, I.; Sheves, M.; Cahen, D. Proteins as Electronic Materials: Electron Transport through Solid-State Protein Monolayer Junctions. *J. Am. Chem. Soc.* **2010**, *132*, 4131–4140.
15. He, T.; Friedman, N.; Cahen, D.; Sheves, M. Bacteriorhodopsin Monolayers for Optoelectronics: Orientation and Photoelectric Response on Solid Supports. *Adv. Mater.* **2005**, *17*, 1023–1027.
16. Jin, Y. D.; Friedman, N.; Sheves, M.; Cahen, D. Bacteriorhodopsin-Monolayer-Based Planar Metal–Insulator–Metal Junctions *via* Biomimetic Vesicle Fusion: Preparation, Characterization, and Bio-optoelectronic Characteristics. *Adv. Funct. Mater.* **2007**, *17*, 1417–1428.
17. Sepunaru, L.; Friedman, N.; Pecht, I.; Sheves, M.; Cahen, D. Temperature-Dependent Solid-State Electron Transport through Bacteriorhodopsin: Experimental Evidence for Multiple Transport Paths through Proteins. *J. Am. Chem. Soc.* **2012**, *134*, 4169–4176.
18. Jin, Y. D.; Honig, T.; Ron, I.; Friedman, N.; Sheves, M.; Cahen, D. Bacteriorhodopsin as an Electronic Conduction Medium for Biomolecular Electronics. *Chem. Soc. Rev.* **2008**, *37*, 2422–2432.
19. Jin, Y. D.; Friedman, N.; Sheves, M.; Cahen, D. Effect of Metal–Molecule Contact Roughness on Electronic Transport: Bacteriorhodopsin-Based, Metal–Insulator–Metal Planar Junctions. *Langmuir* **2008**, *24*, 5622–5626.
20. Patil, A. V.; Premaraban, T.; Berthoumieu, O.; Watts, A.; Davis, J. J. Engineered Bacteriorhodopsin: A Molecular Scale Potential Switch. *Chem.—Eur. J.* **2012**, *18*, 5632–5636.
21. Patil, A. V.; Premaruban, T.; Berthoumieu, O.; Watts, A.; Davis, J. J. Enhanced Photocurrent in Engineered Bacteriorhodopsin Monolayer. *J. Phys. Chem. B* **2011**, *116*, 683–689.
22. Zhao, J.; Davis, J. J.; Sansom, M. S. P.; Hung, A. Exploring the Electronic and Mechanical Properties of Protein Using Conducting Atomic Force Microscopy. *J. Am. Chem. Soc.* **2004**, *126*, 5601–5609.
23. Berthoumieu, O.; Patil, A. V.; Xi, W.; Aslimovska, L.; Davis, J. J.; Watts, A. Molecular Scale Conductance Photoswitching in Engineered Bacteriorhodopsin. *Nano Lett.* **2011**, *12*, 899–903.
24. Milder, S. J.; Thorgeirsson, T. E.; Miercke, L. J. W.; Stroud, R. M.; Kliger, D. S. Effects of Detergent Environments on the Photocycle of Purified Monomeric Bacteriorhodopsin. *Biochemistry* **1991**, *30*, 1751–1761.
25. Hartsel, S. C.; Cassim, J. Y. Structure and Photodynamics of Bacteriorhodopsin in a Delipidated Contracted Lattice form of Purple Membrane. *Biochemistry* **1988**, *27*, 3720–3724.
26. Heyes, C. D.; El-Sayed, M. A. The Role of the Native Lipids and Lattice Structure in Bacteriorhodopsin Protein Conformation and Stability as Studied by Temperature-Dependent Fourier Transform-Infrared Spectroscopy. *J. Biol. Chem.* **2002**, *277*, 29437–29443.
27. Luecke, H.; Schobert, B.; Richter, H.-T.; Cartailler, J.-P.; Lanyi, J. K. Structure of Bacteriorhodopsin at 1.55 Å Resolution. *J. Mol. Biol.* **1999**, *291*, 899–911.
28. Woutersen, S.; Hamm, P. Time-Resolved Two-Dimensional Vibrational Spectroscopy of a Short α-Helix in Water. *J. Chem. Phys.* **2001**, *115*, 7737–7743.
29. Cohen, S. R.; Kalfon-Cohen, E. Dynamic Nanoindentation by Instrumented Nanoindentation and Force Microscopy: A Comparative Review. *Beilstein J. Nanotechnol.* **2013**, *4*, 815–833.
30. Zaccai, G. How Soft Is a Protein? A Protein Dynamics Force Constant Measured by Neutron Scattering. *Science* **2000**, *288*, 1604–1607.
31. Zhang, M.; Wu, Y. Pressure-Induced Structural and Hydration Changes of Proteins in Aqueous Solutions. *Anal. Sci.* **2011**, *27*, 1139–1139.

32. Della Pia, E. A.; Macdonald, J. E.; Elliott, M.; Jones, D. D. Direct Binding of a Redox Protein for Single-Molecule Electron Transfer Measurements. *Small* **2012**, *8*, 2341–2344.
33. Li, W.; Sepunaru, L.; Amdursky, N.; Cohen, S. R.; Pecht, I.; Sheves, M.; Cahen, D. Temperature and Force Dependence of Nanoscale Electron Transport *via* the Cu Protein Azurin. *ACS Nano* **2012**, *6*, 10816–10824.
34. Pan, Y.; Brown, L.; Konermann, L. Hydrogen Exchange Mass Spectrometry of Bacteriorhodopsin Reveals Light-Induced Changes in the Structural Dynamics of a Biomolecular Machine. *J. Am. Chem. Soc.* **2011**, *133*, 20237–20244.
35. Arun, N.; Mukhopadhyay, S.; Narayan, K. S. Monitoring Intermediate States of Bacteriorhodopsin Monolayers Using Near-Field Optical Microscopy. *Appl. Opt.* **2010**, *49*, 1131–1138.
36. Das, A. J.; Mukhopadhyay, S.; Narayan, K. S. Characteristic Noise Features in Light Transmission across Membrane Protein Undergoing Photocycle. *J. Chem. Phys.* **2011**, *134*, 075101-1–075101-5.
37. Jin, Y.; Friedman, N.; Sheves, M.; He, T.; Cahen, D. Bacteriorhodopsin (bR) as an Electronic Conduction Medium: Current Transport through bR-Containing Monolayers. *Proc. Natl. Acad. Sci. U.S.A.* **2006**, *103*, 8601–8606.
38. Lewis, A.; Rousso, I.; Khachatryan, E.; Brodsky, I.; Lieberman, K.; Sheves, M. Directly Probing Rapid Membrane Protein Dynamics with an Atomic Force Microscope: A Study of Light-Induced Conformational Alterations in Bacteriorhodopsin. *Biophys. J.* **1996**, *70*, 2380–2384.
39. Váró, G.; Lanyi, J. K. Distortions in the Photocycle of Bacteriorhodopsin at Moderate Dehydration. *Biophys. J.* **1991**, *59*, 313–322.
40. Korenstein, R.; Hess, B. Hydration Effects on the Photocycle of Bacteriorhodopsin in Thin Layers of Purple Membrane. *Nature* **1977**, *270*, 184–186.
41. Aharoni, A.; Ottolenghi, M.; Sheves, M. Photoreduction of Bacteriorhodopsin Schiff Base at Low Humidity. A Study with C_{13}═C_{14} Nonisomerizable Artificial Pigments. *Photochem. Photobiol.* **2002**, *75*, 668–674.
42. Grudinin, S.; Büldt, G.; Gordeliy, V.; Baumgaertner, A. Water Molecules and Hydrogen-Bonded Networks in Bacteriorhodopsin Molecular Dynamics Simulations of the Ground State and the M-Intermediate. *Biophys. J.* **2005**, *88*, 3252–3261.
43. Lehnert, U.; Réat, V.; Weik, M.; Zaccaï, G.; Pfister, C. Thermal Motions in Bacteriorhodopsin at Different Hydration Levels Studied by Neutron Scattering: Correlation with Kinetics and Light-Induced Conformational Changes. *Biophys. J.* **1998**, *75*, 1945–1952.
44. Leary, E.; Höbenreich, H.; Higgins, S. J.; van Zalinge, H.; Haiss, W.; Nichols, R. J.; Finch, C. M.; Grace, I.; Lambert, C. J.; McGrath, R.; *et al*. Single-Molecule Solvation-Shell Sensing. *Phys. Rev. Lett.* **2009**, *102*, 086801.
45. Garczarek, F.; Gerwert, K. Functional Waters in Intraprotein Proton Transfer Monitored by FTIR Difference Spectroscopy. *Nature* **2006**, *439*, 109–112.
46. Luecke, H.; Schobert, B.; Richter, H.-T.; Cartailler, J.-P.; Lanyi, J. K. Structural Changes in Bacteriorhodopsin During Ion Transport at 2 Angstrom Resolution. *Science* **1999**, *286*, 255–260.
47. Lin, J.; Balabin, I. A.; Beratan, D. N. The Nature of Aqueous Tunneling Pathways between Electron-Transfer Proteins. *Science* **2005**, *310*, 1311–1313.
48. Papadopoulos, G.; Dencher, N. A.; Zaccai, G.; Biildt, G. Water Molecules and Exchangeable Hydrogen Ions at the Active Centre of Bacteriorhodopsin Localized by Neutron Diffraction Elements of the Proton Pathway?. *J. Mol. Biol.* **1990**, *214*, 15–19.